

Loop modeling of coronal X-ray spectra

IV. One- and two-loop model fitting of ROSAT PSPC spectra: three test cases

A. Maggio and G. Peres

Istituto e Osservatorio Astronomico, Palazzo dei Normanni, I-90134 Palermo, Italy
(maggio@oapa.astropa.unipa.it, gperes@oapa.astropa.unipa.it)

Received 16 January 1997 / Accepted 6 March 1997

Abstract. We present a detailed application of coronal hydrostatic loop models to fit ROSAT/PSPC X-ray spectra, using three late-type stars, Procyon (F5 IV - V), ι Vir (F6 III), and HR 3625 (F9 V), selected as test cases showing different activity levels. We present results of the spectral analysis with models of coronae made of one class of loops or two classes of loops, and compare them with the results obtained with two-component isothermal models. The loop model analysis is performed with a χ^2 fitting method as accurate as in the case of the two-temperature modeling, including evaluation of statistical confidence regions in the model parameter space. We show that the observed spectra of Procyon and ι Vir can be successfully fitted with one-loop models, while two-loop models are required to fit the spectrum of HR 3625. In the case of Procyon, for which EUVE spectra are also available, we find that a coronal density estimate – based on emission line ratios – is consistent with the results of our one-loop model fitting. The case of HR 3625 is adopted to illustrate how the confidence regions in the two-loop model parameter space can be explored and interpreted. Our final results indicate different coronal conditions for the three selected stars: Procyon emission is dominated by relatively short ($L \sim 10^9$ cm), low pressure ($p_0 \sim 2$ dyn cm $^{-2}$) and low temperature ($T_{\max} = 1.7 \times 10^6$ K) loops, covering few tens percent of the stellar surface; the corona of ι Vir appears composed of relatively higher pressure ($p_0 = 2$ – 10 dyn cm $^{-2}$), higher temperature ($T_{\max} = 1$ – 2×10^7 K) loops with height ($L = 1$ – 6×10^{10} cm) comparable with the pressure scale height; finally, the coronal emission of HR 3625 can be modelled with low-temperature ($T_{\max} = 1$ – 2×10^6 K), short ($L < 5 \times 10^8$ cm) loops, with base pressure $p_0 > 6$ dyn cm $^{-2}$, possibly covering a large fraction of the stellar surface, plus higher temperature ($T_{\max} > 7 \times 10^6$ K) loops which may range from compact, very active region loops ($L < 10^9$ cm, $p_0 > 10^2$ dyn cm $^{-2}$) covering less than 0.5% of the surface, to larger, relatively less active region loops ($L \sim 10^{10}$ cm, $p_0 = 5$ – 10 dyn cm $^{-2}$) covering at most 10% of the surface.

Key words: stars: coronae – stars: late-type – X-rays: stars – methods: data analysis

1. Introduction

Despite the increase in sensitivity and spectral resolving power of X-ray instrumentation, the modeling of late-type stars spectra is still largely limited to models with a small number of isothermal components (usually two components) at different temperatures. On the other hand, plasma magnetically confined in coronal arches, with a thermal and density stratification, is widely recognized as the most plausible source of the observed coronal emission at X-ray and EUV wavelengths, in analogy to the Sun, which is characterized by a highly structured corona.

For this reason we have initiated a project dedicated to the analysis and interpretation of stellar X-ray emission with the help of detailed coronal loop models, which have already been tested with success in the interpretation of spatially-resolved observations of the solar corona. This paper is our first application yielding interpretation of observed coronae by means of extensive loop modeling. Such a modeling, theoretically based on reasonably firm grounds, is within the reach of our computation capabilities since a few years ago, but it has not reached enough popularity yet – in our opinion – because of the lack of a clear, conceptual framework which shows what physical insight could be derived from the observed spectra.

To fulfill this scientific need, in the preceding papers of the series we have addressed some fundamental aspects of the “loop modeling” approach. The general properties of our hydrostatic model have been described by Ciaravella et al. (1996; Paper I), while Maggio & Peres (1996; Paper II) have investigated constraints and diagnostics that can be derived from the spectral fitting with loop models; Ciaravella et al. (1997; Paper III) have compared loop model spectra with the one-component (1-T) and the two-component (2-T) isothermal model spectra usually adopted for the analysis of X-ray observations.

The present paper deals with the application of loop modeling to the analysis of real data, and in particular to the fitting of

ROSAT/SPSC X-ray (0.1-2.4 keV) spectra, with an approach based on statistical tests of hypothesis, as accurate and systematic as in the case of the standard 1-T or 2-T model fitting. We have selected three stars, Procyon, ι Vir and HR 3625, as test cases to illustrate some of the complexity of the analysis as well as some scientific results.

Not surprisingly, some high-quality ROSAT/SPSC spectra are not well described by a one-loop model and require a two-loop model fitting. In such cases, the interpretation of the fitting results is complicated because of the high number of dimensions of the parameter space. For this reason, we use the three sample cases to illustrate in detail how one-loop and two-loop model fitting is performed, and how useful diagnostics on the properties of the coronal plasma can be derived from the fitting results. In particular, the case of HR 3625 is relevant to show how the confidence regions in a two-loop model parameter space can be presented and interpreted, based on what has already been learned on the features of one-loop model fitting.

From the point of view of their spectral characteristics and of the results obtained with the loop modeling, we anticipate that the three selected stars are fairly representative of the larger sample of F and G stars which will be the subject of the next two papers in this series.

In Sect. 2 we introduce the stars selected for this work; in Sect. 3 we describe the analysis procedures and we present the results that are discussed in Sect. 4; finally, Sect. 5 is devoted to a summary of the methodological approach and to conclusions.

2. The test cases

The three stars selected for this paper are Procyon (F5 IV - V), ι Vir (F6 III-IV), and HR 3625 (F9 V).

Procyon is a well known, nearby ($D = 3.4$ pc), astrometric binary with a cool white dwarf companion, and it is a good example of a slightly evolved, low-activity X-ray source. It has been already studied in X-rays in the past (Schmitt et al. 1985; Jordan et al. 1986; Lemen et al. 1989), and most recently also in EUV with the Extreme UltraViolet Explorer (EUVE) by Schmitt et al. (1994, 1996), by Drake et al. (1995), and by Schrijver et al. (1995). All the observed X-ray emission is attributable to the F-type primary (Schmitt et al. 1985), so we can ignore the presence of another star as far as the spectral analysis is concerned.

ι Vir ($D = 23$ pc) is an interesting example of a single late-type star, likely in the phase of crossing the Hertzsprung gap (Gilliland 1985), and showing evidence of a moderately high activity level. Its ROSAT/SPSC observation has been already presented by Maggio et al. (1994b).

Finally, HR 3625 is a single late-F main-sequence star located at ~ 22 pc from the Sun, serendipitously observed with ROSAT; the characteristics of its X-ray emission are somewhat intermediate between those of the preceding two objects.

3. Analysis of the X-ray spectra

In Table 1 we have listed some characteristics of the X-ray observations.

Table 1. X-ray data

Object Name	ROSAT/SPSC Observation ID	Off-axis Angle (arcmin)	Livetime (ksec)	Net Counts	Selected energy bins
Procyon #1	200437	1.3	0.8	2586	3:19
Procyon #2	200437	1.4	1.9	6609	3:21
Procyon #3	200437	1.4	1.9	6463	3:21
Procyon #4	201118	1.5	2.8	9330	3:23
ι Vir	200908	0.8	2.7	2134	3:28
HR 3625	700326	44.1	14.5	2267	3:26

Two observations of Procyon are available in the public ROSAT archive: the first one comprises two exposures, separated by about one year; the second observation has been performed 6 months after the end of the first one. From these two observations we have extracted four spectra, taken at different epochs, with less than 10^4 counts each, that we have analyzed separately.¹ There is significant variability (at the 99% confidence level) in the source intensity detected in the data segment #3, according to both the Kolmogorov-Smirnov and the Cramer-von Mises one-sample goodness-of-fit tests, which is associated to a smooth variation of the count rate throughout the observation time window. Some marginal variability (90% confidence level) is also present in the data segment #1. Significant variability was detected also in the 14.5 ksec observation of HR 3625, spanning 7 days, but in none of these cases there is evidence of flare-like events. This variability is not due to instrumental effects, in fact it is not detected in the background light curve, and it does not appear associated with significant changes of the shape of the observed spectra.

For the on-axis sources (Procyon and ι Vir) the source spectrum was extracted from a circular region of $2'$, and the background was evaluated in an annulus of $3'$ and $6'$ inner and outer radii, respectively. For the off-axis source HR 3625, we have used a source radius of $4'$ and a background annulus between $5'$ and $8'$, to take into account the larger width of the PSF. We have also checked that the “ribs” of the detector window do not mask the source region (the nearest rib being at $8'$ from the X-ray source position).

We have analyzed each observed spectrum with several models: a *2-T model*, which is the most widely used for fitting stellar X-ray spectra; a *single-loop model*, with an optional expanding loop cross-section, and a *two-loop model* whenever the data required such a more complex analysis. For all models we have adopted the Raymond & Smith (1977) plasma emis-

¹ The analysis of ROSAT/SPSC spectra with a larger number of counts is likely dominated by the uncertainties in the spectral response of the instrument rather than by the statistical errors. In fact, when the number of counts in the most populated energy bins of the instrument exceeds $\sim 2 \times 10^3$, their relative error due to Poisson statistics becomes comparable to the 2% systematic error (not included in our analysis) estimated by Fiore et al. (1994) and by Bocchino et al. (1994) to take into account residual uncertainties in the spectral calibration.

sivities (computed with the code, version 1989, kindly provided to us by J. Raymond), assuming solar abundances (Anders & Grevesse 1989). We note in passing that the limited spectral resolution of the ROSAT/PSPC does not warrant tackling with the effects that different emissivity codes or slight changes in the plasma abundances may have on the fitted model parameters; however, these issues may become important in the analysis of spectra with higher spectral resolution, as those obtained with the instrumentation on board the ASCA satellite.

The source and background spectrum extraction was carried out within the IRAF/PROS V2.4 environment, while the rest of the analysis, including the spectral fitting, has been performed with the Analysis System for Astrophysical Plasmas (ASAP; Maggio et al. 1994a). The ASAP results of the fitting with the 2-T model have also been checked for consistency using the better known packages for spectral analysis XSPEC and the one in IRAF/PROS. In all cases the 1σ uncertainties on the observed net counts were computed according to the approximation of Gehrels (1986) for Poisson-distributed deviates, and the goodness of the fit was tested using the χ^2 statistics by adopting the threshold value at the 90% confidence level for the appropriate number of degrees of freedom (d.o.f.). For the fitting, we have always excluded the first two PSPC energy channels, in the standard 34-bin scheme, and all the high energy channels with less than five photons per bin, because they are the most affected by background fluctuations and because they may not contribute properly to the χ^2 statistics.

Confidence regions in the subspace of the interesting parameters for each model have been computed according to the prescription of Lampton et al. (1976) for composite hypothesis tests.

3.1. Analysis with a two-temperature model

The 2-T model is characterized by four free parameters, two temperatures, T_1 and T_2 , and two normalizations, k_1 and k_2 , with $k_i = EM_i/4\pi D^2$, where $EM = \int n_e^2 dV$ is the plasma volume emission measure, and D is the source distance. Since all the stars we considered are relatively nearby ($D < 25$ pc), as a first guess we have fixed the ISM hydrogen column density, N_H , to the value computed from the trigonometric parallax assuming an hydrogen number density of 0.07 cm^{-3} , typical of the local ($D < 100$ pc) interstellar medium (Paresce 1984). For Procyon we have adopted the value $N_H = 10^{18} \text{ cm}^{-2}$ also reported by Paresce (1984). This choice is preferable in order to reduce the number of free parameters. In one case (HR 3625) the fitting residuals showed an excess of the model with respect to the data in the softest instrument energy channels, although the χ^2 was acceptable, indicating more absorption than expected. In this case, we have repeated the analysis with a N_H value of $5 \times 10^{19} \text{ cm}^{-2}$, i.e. 10 times greater, and we have obtained a lower χ^2 and a better distribution of the residuals. The same approach has been followed for the analysis with the loop models, and we have observed the same behavior.

The results of the analysis with the 2-T model are reported in Table 2, the observed spectra and 2-T best-fit models are

shown in Fig. 1. For Procyon we show only the results relative to one data segment (#3), since they are similar for the other segments. For HR 3625 we show the results obtained assuming $N_H = 5 \times 10^{19} \text{ cm}^{-2}$.

The 2-T model yields acceptable χ^2 values for all the spectra analyzed. The results suggest that the three stars may have coronae with very different plasma characteristics. The very soft Procyon's spectrum, with little differences between the various data segments, can be essentially described by a dominant low-temperature component ($T_1 \sim 1 \times 10^6$ K) with a volume emission measure $EM \sim 9 \times 10^{50} \text{ cm}^{-3}$, and a second component, whose temperature is poorly constrained by the fitting (see Table 2), with 10-20% of the EM of the cool component, and contributing only 5-10% of the observed counts. Note that in the sole case of the data segment #1 of Procyon, a one-component isothermal model is adequate to describe the observed spectrum (see Table 2): the higher temperature component is not required to fit the data segment #1, likely because the number of counts is relatively lower than in other segments. At the other extreme, the 2-T model fitting of ι Vir indicates that the EM of the hot-temperature component ($T_2 \sim 9 \times 10^6$ K) is about twice that of the cool component ($T_1 \sim 2 \times 10^6$ K, $EM \sim 4 - 6 \times 10^{51} \text{ cm}^{-3}$). In the case of HR 3625, instead, the coronal EM is dominated by the cool component ($EM_2/EM_1 = 0.3 - 0.5$), the two temperatures being similar to those of ι Vir.

3.2. One-loop modeling

We have used the enhanced version of the Serio et al. (1981) hydrostatic coronal loop model, described in Paper I. Here we just recall that the plasma is described as a compressible fluid in hydrostatic equilibrium under the effect of gravity, and with energy balance between the heat input, optically thin radiative losses and thermal conduction.

The loop model is characterized by three free parameters: two of them can be chosen among the plasma pressure, p_0 , at the base of the loop (where $T = 2 \times 10^4$ K), the loop semi-length, L , and the plasma maximum temperature, T_{max} , at the loop apex; in fact, these three quantities are linked together by the Serio et al. (1981) scaling law (see also Paper II). The third free parameter is a normalization factor, which can be expressed as

$$k = fq(L/R_*) \left(\frac{R_*}{D} \right)^2 \quad (1)$$

where f is the surface filling factor, i.e. the fraction of the stellar surface covered by the loop footpoints, and $q(L/R_*)$ is a geometric factor which takes into account the fraction of the X-ray emitting volume obscured by the stellar disk, assuming spherical symmetry (Schmitt 1990; Giampapa et al. 1996; Jordan 1996)

$$q(x) = \frac{1}{2x} \left[x + x^2 + \frac{x^3}{3} + \frac{1}{3}(2x + x^2)^{3/2} \right] \quad (2)$$

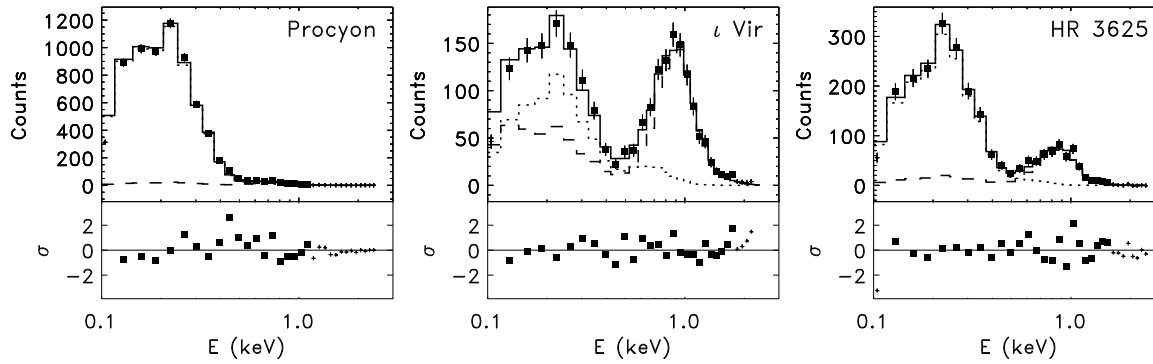


Fig. 1. Upper panels: ROSAT PSPC spectra of the sample stars and best-fit 2-T models. Dotted and dashed lines indicate the contribution due to the cool and the hot component, respectively; the total spectrum is represented with a solid line. The spectrum of Procyon is relative to the data segment #3 (see Table 1). The best-fit model for HR 3625 is the one obtained assuming $N_{\text{H}} = 5 \times 10^{19} \text{ cm}^{-2}$ (see Table 2). Lower panels: differences between models and data divided by the errors

Table 2. 2-T model fitting results. The 90% confidence ranges have been computed with the criterion $\chi^2 < \chi^2_{\text{min}} + 4.61$ (Lampton et al. 1976). In few cases the best-fit value is equal to one of the range boundaries because of the finite resolution of the model grid used for the χ^2 fitting.

Name	N_{H} cm^{-2}	T_1 10^6 K	90% conf. range		EM_1 10^{50} cm^{-3}	90% conf. range		T_2 10^6 K	90% conf. range		$\frac{EM_2}{EM_1}$	90% conf. range		χ^2_{r}	d.o.f.
Procyon	$1 \cdot 10^{18}$														
#1		1.3			9.5									1.1	15
#1		1.1	0.7	1.3	7.8	2.3	9.4	2.2	> 1.4	0.20	> 0.03	0.5	13		
#2		1.1	1.1	1.3	8.6	8.2	9.5	3.2	3.5	11.2	0.08	0.02	0.13	1.2	15
#3		1.1	1.1	1.3	8.3	7.7	9.4	2.5	2.0	8.9	0.12	0.02	0.23	0.8	15
#4		1.1	1.1	1.3	7.9	7.4	9.3	2.2	2.0	7.1	0.17	0.02	0.25	1.1	17
$\iota \text{ Vir}$	$5 \cdot 10^{18}$	2.0	1.6	2.2	48.2	37.5	58.4	8.9	7.9	8.9	2.13	1.40	2.91	0.6	22
HR 3625	$5 \cdot 10^{18}$	1.6	1.6	1.8	24.4	24.2	26.7	7.9	7.1	8.9	0.44	0.33	0.53	0.8	20
	$5 \cdot 10^{19}$	1.3	1.3	1.4	30.8	30.1	32.4	7.1	5.6	8.9	0.37	0.33	0.46	0.7	20

The procedure of folding the emitted loop spectrum with the instrument response, and the χ^2 fitting method has been described in detail in Paper II. At variance with the latter work, we have preferred to search for the best-fit model over a set of 50×20 models (hereafter grid models) in the $T_{\text{max}} - L$ parameter space (instead of the $p_0 - L$ space), spanning the ranges $\log T_{\text{max}}(\text{K}) = [6.0, 7.47]$ and $\log L(\text{cm}) = [8.15, 12.9]$ at equal steps in the logarithm. The advantages of this choice will be clear below.

In order to compute the loop model, an estimate of the stellar radius and gravity is required (which enter in the computation of the hydrostatic equilibrium). In the case of Procyon we have adopted the stellar parameters reported in Schmitt et al. (1985); for $\iota \text{ Vir}$ we have estimated the mass by interpolating between the evolutionary tracks of Maeder and Meynet (1988), and the radius by using the Barnes-Evans relation (Barnes et al. 1978); finally, for HR 3625 we have adopted the standard values for a G0V star reported in Allen (1973), since this star lies close to the main-sequence. In any case, we have checked that slight variations ($\sim 10\%$) in the stellar parameters do not affect significantly our results.

In Paper II we have shown that our ability to constrain the loop model parameters depends on the distribution of the plasma emission measure vs. temperature. More specifically, for loops significantly below the pressure scale height, the spectral fitting allows us to constrain well the plasma peak temperature and hence the product of the base pressure with the loop semi-length, but not each of the two separately. This is a fundamental property of loop models, due to a scale invariance of the equations describing the hydrostatic loop model with uniform plasma pressure (see also Serio 1995). Instead, for input loops with lengths of the order of the pressure scale height or larger, the spectral fitting yields closed confidence regions in the parameter space, allowing us to constrain the loop parameters, with different levels of discrimination depending on the photon counting statistics, and on the instrument energy response.

The results of the one-loop model fitting are reported in Table 3, and will be described and discussed in Sect. 4.

3.3. Two-loop modeling

The diagnostic aspects described in the previous section apply in the assumption that a single class of loops dominates the

Table 3. One-loop modeling results. The 90% confidence ranges have been computed with the criterion $\chi^2 < \chi^2_{\min} + 4.61$ (Lampton et al. 1976). In few cases the best-fit value is equal to one of the range boundaries because of the finite resolution of the model grid used for the χ^2 fitting.

Name	N_H cm^{-2}	p_0 $dyn\ cm^{-2}$	90% conf. range	L $10^{10}\ cm$	90% conf. range	T_{max} $10^6\ K$	90% conf. range	Filling Factor	90% conf. range	χ^2_r	d.o.f.
Procyon	$1\ 10^{18}$										
#1		10.0	> 0.4	0.03	< 0.56	1.7	1.6 - 2.0	0.05	< 1.82	0.8	14
#2		7.9	> 0.3	0.03	< 0.56	1.61	1.56 - 1.70	0.07	< 2.04	2.3	16
#3		8.9	> 0.2	0.03	< 1.00	1.68	1.68 - 1.76	0.06	< 3.40	1.4	16
#4		8.9	> 0.6	0.03	< 0.32	1.68	1.68 - 1.73	0.06	< 1.06	1.7	18
$\iota\ Vir$	$5\ 10^{18}$	3.2	2.0 - 10.0	25.0	6.3 - 63.1	12.9	11.1 - 17.3	0.09	0.04 - 0.12	0.8	23
HR 3625	$5\ 10^{18}$	1.2	1.1 - 1.4	793.4	> 44.5	23.2	> 10.1	0.001	< 0.29	2.3	21
	$5\ 10^{19}$	0.8	0.7 - 0.9	793.5	> 79.4	19.9	> 10.4	0.004	< 0.28	1.9	21

disk-integrated stellar X-ray emission. But the analogy with the solar corona suggests that coronal emission may well originate from an ensemble of loops with different characteristics. Two-loop modeling is the natural step forward if the one-loop model does not yield acceptable results, as much as the 2-T model is adopted if the 1-T fitting fails. We have resorted to the two-loop modeling only when such a modeling is warranted by the data quality, and the one-loop model fitting has failed.

The main difficulty with two-loop modeling rests in the exploration of the six-dimensional parameter space, and the related construction and visualization of statistical confidence regions. This is not simply a matter of adequate computational power, but also a problem of identification of the relevant parameters for an efficient search of the best-fit model and a clear interpretation of the fitting results.

First, note that the normalizations (see Eq. 1) of the two loop components can be both computed analytically, once all the other parameters have been determined. In fact, the χ^2 statistic assumes a quadratic form as a function of these normalizations, k_1 and k_2 :

$$\chi^2 = \sum \left(\frac{O_j - k_1 C_{1,j}(T_{1max}, L_1) - k_2 C_{2,j}(T_{2max}, L_2)}{\sigma_j} \right)^2 \quad (3)$$

where O_j are the observed counts in the j -th instrument channel, σ_j the related 1σ errors, $C_{1,j}$ and $C_{2,j}$ the non-normalized predicted counts for the two loop model components, with assigned T_{max} and L . It can be shown with some algebra that a global minimum χ^2 exists for real, *non-negative* values² of k_1 and k_2 . It follows that it is sufficient to search for the best-fit solution by computing the χ^2 in each of the ‘‘points’’ identified by the other four parameters, T_{1max} , T_{2max} , L_1 , L_2 , assuming

² The normalizations can be simply computed as in the general linear least squares problem (described, e.g., in Press et al. 1986), with the caveat that solutions with either $k_1 < 0$ or $k_2 < 0$ are not physical, and in such cases the minimum χ^2 value is found by resetting $k_1 = 0$ or $k_2 = 0$, respectively.

the values of the model grid defined in Sect. 3.2, and then find out k_1 and k_2 .

Moreover, note that for loops shorter than the pressure scale height, the effective dimensionality of the parameter space is reduced: as recalled above, T_{max} is the only parameter which determines the spectral shape, while p_0 and L are, in practice, not individually important. This is one of the reasons for the choice of a T_{max} - L model grid.

In the following section, we will illustrate the possible fitting solutions in a two-loop model parameter space, with the help of a specific example (see Sect. 4.3).

4. Loop modeling applications, results and discussion

4.1. Procyon: loops shorter than the pressure scale height

We have found acceptable (at the 90% confidence level) best-fit one-loop models for two out of four of the Procyon’s spectra, namely for the data segments #1 (~ 2600 counts) and #3 (~ 6500 counts). The other two data sets have more counts (~ 6600 counts in the segment #2, and ~ 9300 counts in the segment #4), and the relatively poor fits may be attributed, at least in part, to the higher photon counting statistics, since systematic errors have not been taken into account (see Sect. 3). On the other hand, the best-fit loop parameters are remarkably similar in all cases, analogously to what occurred when fitting with the 2-T model, and in line with the constancy of the X-ray luminosity ($L_X = 1.9 \times 10^{28}$ erg s $^{-1}$) over the long time interval spanned by the observations (> 1.5 yr). For these reasons, we will focus the attention on the analysis of the data segment #3, because of its relatively high photon statistic and the good quality of the fit.

The Procyon spectrum is best-fitted with models of loops shorter than one pressure scale height ($s_p \sim 2 \times 10^{10} T_6$ cm, characterized by $\log T_{max} = 6.20 - 6.27$ K, hence p_0 and L cannot be independently constrained. Considering that the integrated emission of one loop scales roughly as $p_0^2 L$, and $p_0 L \sim T_{max}^3$ (Rosner et al. 1978), the constraint on T_{max} and the indetermination on p_0 do not allow to constrain the surface filling factor, since the total coronal luminosity is $\propto p_0^2 L f$;

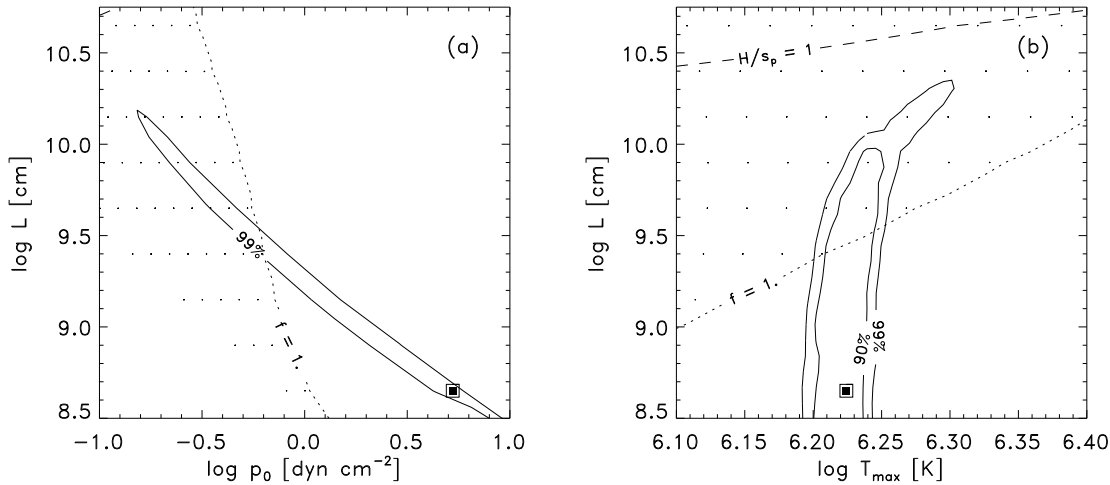


Fig. 2. **a** Confidence region at the 99% level in the $p_0 - L$ plane of the loop parameter space, for Procyon (data segment #3). The square indicates the best-fit loop model. The forbidden region with surface filling factor larger than 1 is shaded. **b** Confidence regions, at the 90% and 99% confidence level, in the $T_{\max} - L$ plane, best-fit model location and forbidden region as in **a**. The dashed line indicate the locus where the loop height, H , is equal to the pressure scale height, s_p , at $T = T_{\max}$. Note that the analogous locus in the plot **a** is mostly outside the upper boundary

however the condition $f \leq 1$ along with the constraint on T_{\max} yield $p_0 > 0.7 \text{ dyn cm}^{-2}$ and $L < 3 \times 10^9 \text{ cm}$.

In Fig. 2 we show the statistical confidence regions relevant for different parameter pairs: in the $p_0 - L$ plane (Fig. 2a) the confidence regions span a wide range of values for both parameters, while in the $T_{\max} - L$ plane (Fig. 2b) the narrow range of allowed T_{\max} values is better appreciated. The latter description is certainly preferable to characterize coronal sources with loops shorter than the pressure scale height. Note also the bending of the confidence region toward higher T_{\max} values for increasing loop lengths: this feature is due to the relative lack of high temperature plasma in model loops with height comparable with the pressure scale height (see the differential emission measure distributions in Fig. 7 of paper II), with respect to shorter loops with the same T_{\max} ; hence, in order to fit the observed spectrum with long loop models, larger T_{\max} values are required. This shape of the confidence regions is typical when the $T_{\max} - L$ plane is adopted, and it will be crucial to understand the space of the allowed solutions when a 2-loop model is employed (see Sect. 4.3).

An early version of loop modeling was performed by Schmitt et al. (1985) on an *Einstein Observatory* IPC spectrum of Procyon. They found $\log T_{\max}$ well constrained in the range 6.36–6.42 K, only slightly larger than our estimate, but p_0 and L separately unconstrained, similarly to what we reported above. More recently, using density-sensitive iron lines (Fe IX – Fe XIV) observed with EUVE, Schmitt et al. (1994, 1996) derived an average coronal density of $n_e = 3 \times 10^9 \text{ cm}^{-3}$ at $T \sim 2 \times 10^6 \text{ K}$ (the peak of their differential emission measure distribution). These two values allow to compute a plasma pressure $p = 1.7 \text{ dyn cm}^{-2}$ which singles out a loop model – among those in the 90% confidence region derived with our analysis (Fig. 2) – with $L = 1.1 \times 10^9 \text{ cm}$, and $f = 0.3$. An independent analysis of the Procyon’s EUV spectrum by Drake

et al. (1995) shows a continuous emission measure distribution over the temperature range $\log T = 5.4 - 6.3$, compatible with that predicted by our loop models.

The above comparison shows that our loop modeling yields results consistent with those independently derived from EUV data, and that plasma density estimates based on these data allow to constrain effectively all the coronal loop parameters.

It’s worth noting that, beyond providing good results, loop model fitting of X-ray spectra, with the additional information derived by EUV data, turns out to be a powerful approach to constrain the characteristics of stellar coronae, at least in cases like the Procyon’s one. Such physical insight cannot be effectively extracted from 2-T fitting results, unless ad-hoc hypotheses on the density and thermal coronal structure are adopted.

In absence of independent estimates of the coronal density, available for many stars observed with EUVE, the loop modeling diagnostics of Procyon-like coronal sources are limited by the solution degeneracy described above: for short, nearly-isobaric loops, the distribution of temperature, and hence the emitted spectrum, are independent of loop length and base pressure (see also Paper II), so that the role of these latter two quantities cannot be disentangled. On the other hand, the plasma maximum temperature and hence the full, scale-invariant temperature distribution are well constrained by the shape of the spectrum.

In summary, Procyon appears as a steady, low-level X-ray source, likely characterized by relatively short, medium-pressure (with respect to the Sun) coronal loops, covering few tens percent of the stellar surface.

4.2. ι Vir: loops as large as the pressure scale height

The case of ι Vir, instead, is representative of a class of one-loop model fitting solutions which are not degenerate. In fact,

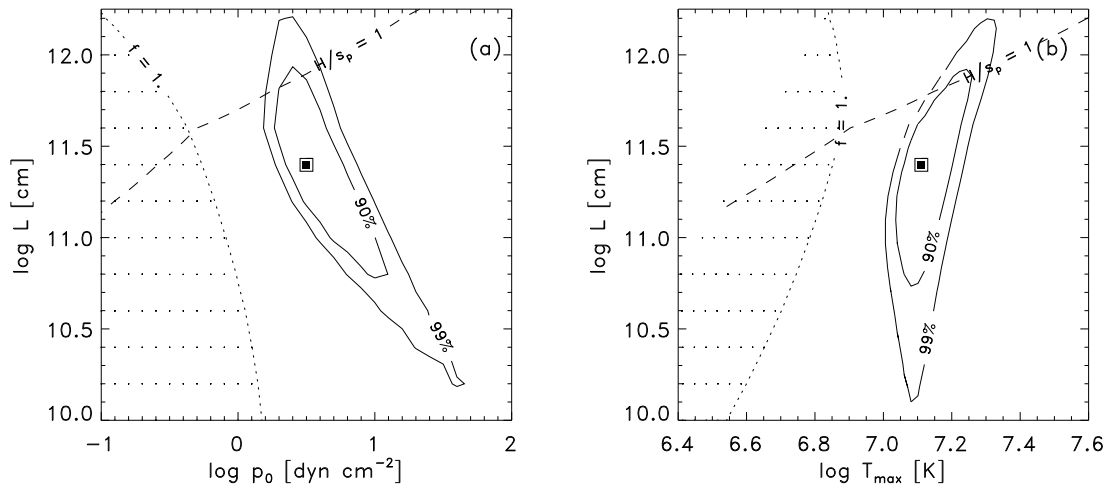


Fig. 3a and b. Confidence regions at the 90% and 99% level in the $p_0 - L$ plane (a) and in the $T_{\max} - L$ plane (b) of the loop parameter space, for ι Vir. The dashed line indicates the locus where the loop height is equal to the pressure scale height at the maximum temperature. The presentation is similar to that of Fig. 3 for other respects

the successful best-fit model indicates loops as large as the pressure scale height, for which the plasma cannot be considered isobaric. In such cases, the effect of gravity in the hydrostatic equation becomes important, and the resulting distribution of the differential emission measure vs. temperature is such that loop modeling of ROSAT/PSPC data yields closed confidence regions, i.e. it allows to constrain all the loop parameters (compare the simulations of Paper II and the results in Fig. 3). For this kind of stellar coronae, if X-ray spectra with sufficiently high signal-to-noise ratio are available, the loop model fitting approach reaches its best diagnostic power.

The corona of this evolved late-type star appears composed of relatively high pressure ($p_0 = 2\text{--}10 \text{ dyn cm}^{-2}$), long loops ($L = 6 \times 10^{10} - 6 \times 10^{11} \text{ cm}$), with maximum plasma temperature $\log T_{\max} = 7.05\text{--}7.24 \text{ K}$, covering from 4% to 12% of the stellar surface.

4.3. HR 3625: from one-loop to two-loop modeling

The analysis of HR 3625 is the most complex in this work, and typical of many other F- and G-type stars that will be presented in the next papers of this series.

The one-loop modeling yields unacceptable χ^2 values (Table 3) irrespective of the N_{H} value assumed. Similar results are obtained by splitting the observation in two or three data segments and analyzing the spectra separately, therefore the inappropriateness cannot be easily ascribed to variability of the source. In Fig. 4 we show the confidence region in the $p_0 - L$ plane to illustrate a feature that we have often found for other stellar spectra, which – in some case – may even yield a χ^2 formally acceptable: the length of the best-fit one-loop model is larger than the pressure scale height, i.e. its base pressure is well constrained, but only a lower limit can be determined for L or T_{\max} . This indetermination is due to two effects: first, for loops longer than the pressure scale height the high-temperature

plasma near the top has very low emission measure, and a further increase in length makes a negligible influence on the emitted spectrum; second, the emission of the plasma with temperature larger than a few $\times 10^7 \text{ K}$ occurs at energies outside the window of the instrument sensitivity. What makes these models unacceptable, irrespective of the χ^2 value, is that the loop height turns out to be orders of magnitude larger than the stellar radius ($L > 10^{12} \text{ cm}$); moreover, in this case, the hydrostatic model hypothesis is not realistic. As an aside, this class of loops is not observed to dominate the emission of the Sun, although we may expect loop populations significantly different in much more active stars.

The failure of the one-loop model fitting could have been guessed from the results of the 2-T fitting, in the light of Paper III: the ratio of the emission measures of the hot vs. the cool isothermal component is less than 1 ($EM_2/EM_1 = 0.4 \pm 0.1 \text{ cm}^{-3}$ for HR 3625; see Table 2), while simulated one-loop spectra fitted with 2-T models invariably yield $EM_2/EM_1 > 1$. The only way for a one-loop model to match a spectrum dominated by relatively low-temperature plasma emission is to have L much larger than the pressure scale height.

As shown in paper III, loop models with expanding cross-section do not represent a solution in such cases. In fact, in these models the amount of high temperature plasma is larger than in constant cross-section loops, so that the effect is the opposite to what is required.

The natural question to ask now is whether some 2-loop models exist which provide a better, and more physically plausible description of the data. A related issue is whether the parameters of such models can be constrained by means of confidence regions. We will show that, in the present case, the answer is definitely yes to the first question and partially yes to the second question.

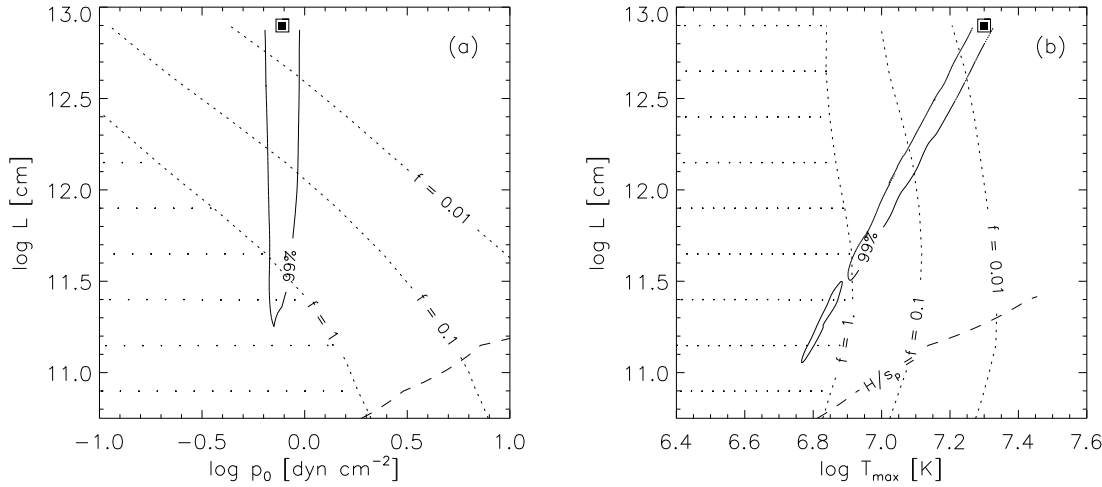


Fig. 4. **a** Confidence regions at the 99% level in the $p_0 - L$ plane of the loop parameter space, for HR 3625. Dotted lines indicate different contour levels for the filling factor. The dashed line indicate the locus where $H = s_p$. Note that the χ^2 associated with the best-fit model (square symbol) is too high to be acceptable: the confidence region is shown only for comparison purposes with the other stars. **b** Similar to **a** but in the $T_{\max} - L$ plane

Table 4. Two-loop modeling sample solutions for HR 3625

Cool-loop component				Hot-loop component				χ_r^2 (18 d.o.f.)	ID
$T_{1\max}$ 10^6 K	p_{01} dyn cm $^{-2}$	L_1 cm	f_1	$T_{2\max}$ 10^6 K	p_{02} dyn cm $^{-2}$	L_2 cm	f_2		
1.7	14.2	2.5×10^8	0.16	10.3	3.1×10^3	2.5×10^8	8.7×10^{-5}	0.8	(a)
1.6	4.3	4.5×10^8	0.86	19.5	7.4	4.5×10^{11}	7.4×10^{-2}	0.9	(b)
1.5	41.9	1.6×10^8	0.17	7.4	5.3	2.8×10^{10}	0.12	1.2	(c)

In Fig. 5a we show the best-fit 2-loop model found by exploration of the 4-dimensional parameter space (the filling factors, f_1 and f_2 , being computed analytically). It is characterized by two classes of loops, both shorter than the pressure scale height ($L_1 = L_2 = 2.5 \times 10^8$ cm), but with quite different base pressure ($p_{01} = 14$ dyn cm $^{-2}$, $p_{02} = 3.1 \times 10^3$ dyn cm $^{-2}$), and maximum temperature ($T_{1\max} = 1.7 \times 10^6$ K, $T_{2\max} = 1.0 \times 10^7$ K), in which the cool loops cover about 16% of the stellar surface and the hot loops a fraction less than 10^{-4} .

The two-loop fitting allows us to get a better physical insight than the one-loop modeling, in this case: the cool loop provides the plasma emission measure at relatively low temperature, missed with one-loop models. The hot-loop plasma pressure (p_{02}) may appear high, especially with respect to the Sun where such a high pressure is typical of loops in flaring conditions. We recall that significant variability has been detected in the X-ray light curve of HR 3625, but with no clear evidence of individual flare-like events. This behavior could be explained with an high frequency of flares, whose superposition may smooth out any large luminosity variation. Thus, the high-pressure loops may simply indicate the persistent occurrence of plasma in flaring state.

Since the only constrained parameter for short loops, from the point of view of the spectral fitting, is their maximum tem-

perature, we can expect to find other 2-loop models with less extreme values of p_0 and larger lengths, which provide an equally acceptable fit to the observed spectrum. One of such alternative solutions is shown in Fig. 5b. A third solution is listed in Table 4 together with the first two.

A comprehensible presentation of the solution space is therefore in order. To visualize the confidence regions we first present and describe the slice in the $T_{\max} - L$ plane of each loop component, obtained by fixing the other loop component at the best-fit position (Fig. 6). Note that the χ^2 contours were drawn at the 68% and 90% confidence levels for four interesting parameters. These figures show that, keeping fixed one of the two loop components, the confidence regions for the other loop component extend from very short, high pressure loops – like the best-fit model – to large, relatively low pressure loops. The shape of the confidence regions is similar to that of the one-loop fitting of the Procyon’s spectrum (Sect. 4.1): for short loops, the confidence regions are almost vertical in the $T_{\max} - L$ plane, i.e. insensitive to variations of the loop height, because the temperature is the only significant parameter; for loops higher than the pressure scale height, the confidence regions bend toward higher T_{\max} values, because of the shape of the differential emission measure for such long loops.

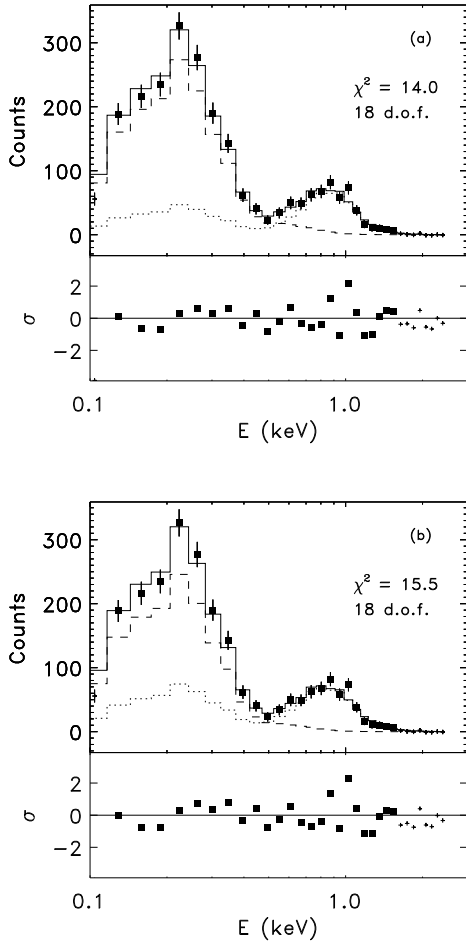


Fig. 5. **a** ROSAT PSPC spectrum of HR 3625 and best-fit 2-loop model, with $T_{1\max} = 1.7 \times 10^6$ K, $p_{01} = 14.2$ dyn cm $^{-2}$, $L_1 = 2.5 \times 10^8$ cm, $f_1 = 0.16$, $T_{2\max} = 1.0 \times 10^7$ K, $p_{02} = 3.1 \times 10^3$ dyn cm $^{-2}$, $L_2 = 2.5 \times 10^8$ cm, $f_2 = 9 \times 10^{-5}$. **b** Alternative acceptable 2-loop model fit, with $T_{1\max} = 1.6 \times 10^6$ K, $p_{01} = 4.3$ dyn cm $^{-2}$, $L_1 = 4.5 \times 10^8$ cm, $f_1 = 0.86$, $T_{2\max} = 2.0 \times 10^7$ K, $p_{02} = 7.4$ dyn cm $^{-2}$, $L_2 = 4.5 \times 10^{11}$ cm, $f_2 = 0.07$

In the same Fig. 6 we have also indicated the regions where the condition on the total filling factor $f = f_1 + f_2 < 1$ is satisfied. Such condition yields a stringent upper limit on the length of the cool loops, $L_1 < 5 \times 10^8$ cm, and hence a lower limit on $p_{01} > 7$ dyn cm $^{-2}$, since $T_{1\max}$ is well constrained in the range $1.3 - 2.1 \times 10^6$ K; the hot component is not constrained by the condition on the filling factor, but a lower limit on the maximum temperature, $T_{2\max} > 7.3 \times 10^6$ K, is determined by the 90% confidence region itself.

Note that models for the cool-loop component which have extremely large lengths ($L_1 > 5 \times 10^{11}$ cm), albeit included in the 90% confidence region and satisfying the condition on the total filling factor, were neglected because they are not physically realistic, as already explained above. A similar argument holds for the longest hot-loop models: we consider as more

physically plausible, a hot loop component whose length does not exceed the pressure scale height, in analogy with the Sun.

In order to explore further the 4-dimensional parameter space, we proceed as follows: first, we consider the 3-dimensional space spanned by the 2-loop parameters $T_{1\max}$, $T_{2\max}$, and L_1 , for a fixed value of L_2 ; in this space we draw an iso- χ^2 surface which confines the 90% confidence level volume; then, we repeat the above two steps for different values of L_2 , thus obtaining a series of 3-D images which shows how the confidence volume changes with this (fourth) parameter; finally, we check where, within the confidence volume, the condition on the total filling factor, $f_1 + f_2 < 1$, is fulfilled. A way of presenting this set of results is through a sequence of images. In Fig. 7 we show four of such images obtained for HR 3625, together with two sections for each confidence volume displayed: the sections in the $T_{1\max} - L_1$ plane are all very similar to the one in Fig. 6, while the sections in the $T_{1\max} - T_{2\max}$ plane show that, for increasing L_2 , the confidence volume moves rigidly toward higher $T_{2\max}$ values; note that the confidence volume does not move appreciably until L_2 becomes sufficiently large, because the spectrum of the hot-loop component is determined only by $T_{2\max}$, and it is almost insensitive to variations of L_2 , as long as the loop remains below the pressure scale height. This behavior is entirely similar for each of the two loop components, as evident from the shape of the confidence regions in Fig. 6.

The above example shows that our ability to constrain 2-loop model parameters is successful in the following respect: with the additional condition on the total surface filling factor, $f_1 + f_2 < 1$, the cool loops are well constrained to maximum temperatures $\log T_{1\max} = 6.2 - 6.3$ K, and semi-lengths $L_1 < 8 \times 10^8$ cm, while for the hot loops we find a lower limit of $\log T_{2\max} > 6.8$ K.

In conclusion, the analysis of the ROSAT/PSPC spectrum of HR 3625 indicates that the corona of this solar-type star can be modelled with two classes of loops (see Table 4): low-temperature, short loops, with base pressure $p_{01} > 6$ dyn cm $^{-2}$, likely covering most of the stellar surface, and high-temperature loops, which may represent either compact, very high-pressure plasma regions ($L_2 < 10^9$ cm, $p_{02} > 10^2$ dyn cm $^{-2}$) covering less than 0.5% of the surface, or longer, high-pressure plasma regions ($L_2 = 10^{10} - 10^{11}$ cm, $p_{02} = 5 - 10$ dyn cm $^{-2}$) covering at most 10% of the surface. As mentioned above, we consider loops much larger than the pressure scale height not physically plausible.

5. Summary and conclusions

We have studied three late-type stars, Procyon, ι Vir, and HR 3625, selected as test cases for their different activity levels, to show how one-loop and two-loop model fitting can be applied to ROSAT/PSPC spectra. Our approach allows to derive constraints on the characteristics of the coronal structures, and hence a better insight on the physics of stellar coronae than usually provided by one- or two-component isothermal models.

We have shown that one-loop models yield successful fits to the X-ray spectra of Procyon and of ι Vir, indicating different

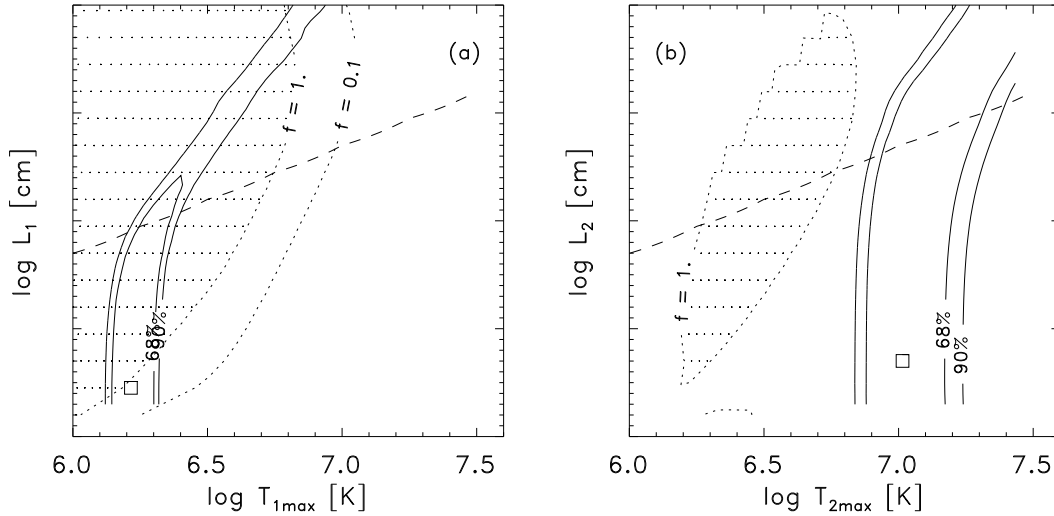


Fig. 6a and b. Confidence regions at the 68% and 90% level in the T_{\max} - L plane, for each component of the 2-loop model, obtained fixing the other loop component at the best-fit location (square symbols). The forbidden region where the total filling factor, $f = f_1 + f_2 > 1$ is shaded. The locus where $f = 0.1$ is also indicated. The dashed lines indicate the loci where $H = s_p$

coronal characteristics: Procyon is a quiet, low-activity source, whose X-ray emission originates from loops shorter than the pressure scale height, for which the plasma temperature distribution can be determined from the analysis of the X-ray data alone, but not the loop length or the plasma pressure at the loop base, due to a scale invariance of the loop model equations; instead, ι Vir is a good example of coronal sources whose emission is dominated by one class of loops with height comparable to the pressure scale height and for which the one-loop modeling is able to provide constraints on all the relevant plasma quantities.

Moreover, in the case of Procyon, we have shown that the one-loop modeling results, beside being satisfactory per-se on the basis of the χ^2 statistic, are also consistent with independent estimates of the coronal plasma density, derived from EUV line ratios. Such estimates are complementary to the X-ray spectral analysis results and can be effectively used to constrain the characteristics of the coronal loop structures, resolving the loop equation degeneracy (scale-invariance) problem.

The case of Procyon has also suggested that, in order to explore and interpret the confidence regions in the loop parameter space, the plasma maximum temperature, T_{\max} , and the loop semi-length, L , are the preferable parameters, T_{\max} being the only well constrained physical parameter for loops shorter than the pressure scale height; this choice allows us to focus effectively on a smaller number of parameters, yet maintaining a complete description. This choice of parameters, together with the interpretation of the shape of the confidence regions for the one-loop modeling case, were applied also to illustrate the features of the two-loop model analysis. A different choice of two parameters, among the not-independent T_{\max} , p_0 , and L , leads to a rather complex and less clear interpretation of the 6-dimensional space of solutions for the two-loop modeling.

A two-loop modeling was required to fit the X-ray spectrum of HR 3625, a late F star whose X-ray emission characteristics are intermediate between those of Procyon and ι Vir, and typical of many other solar-type stars. We have searched the best-fit two-loop model solution by computing the χ^2 in each of the “points” of the 4-dimensional lattice in the parameter space defined by the T_{\max} and L of each loop component. We have then visualized and studied the confidence regions by producing a sequence of 3-D images of the 90% confidence volumes in the $T_{1\max}$ - $T_{2\max}$ - L_1 space, for different values of the fourth parameter, L_2 . Such a sequence of images can be conveniently displayed as a movie, where L_2 plays the role of time. With our approach we can present the results in the space of solutions in a way amenable of a clear interpretation of the physical results. The surface filling factors, f_1 and f_2 , have always been computed analytically, and the condition that the total filling factor, $f_1 + f_2$, must not exceed unity has been exploited to put constraints on the acceptable 2-loop model fitting solutions. We have shown that this approach, in the case of HR 3625, allows us to constrain the characteristics of the cool coronal structures to short loops ($L_1 < 5 \times 10^8$ cm), covering most of the stellar surface, and the hot coronal structures to loops which may be short ($L_2 \sim 10^8$ cm) and with very high plasma pressure ($p_{02} \sim 10^3$ dyn cm $^{-2}$), or longer ($L_2 \sim 10^9 - 10^{10}$ cm), with high plasma base pressure ($p_{02} \sim 10 - 100$ dyn cm $^{-2}$) and covering no more than 10% of the surface. A class of very long loop solutions ($L_2 > 10^{11}$ cm), was excluded on the basis of the physical plausibility.

We stress that our loop modeling approach is quite different from other methods: in the present work we directly fit observations with spectra synthesized from loop models, so as to derive the loop characteristics; instead, in Giampapa et al. (1996) and in Preibisch (1996), for example, the observed spectra are fitted with 2-T or power-law emission measure distributions, then

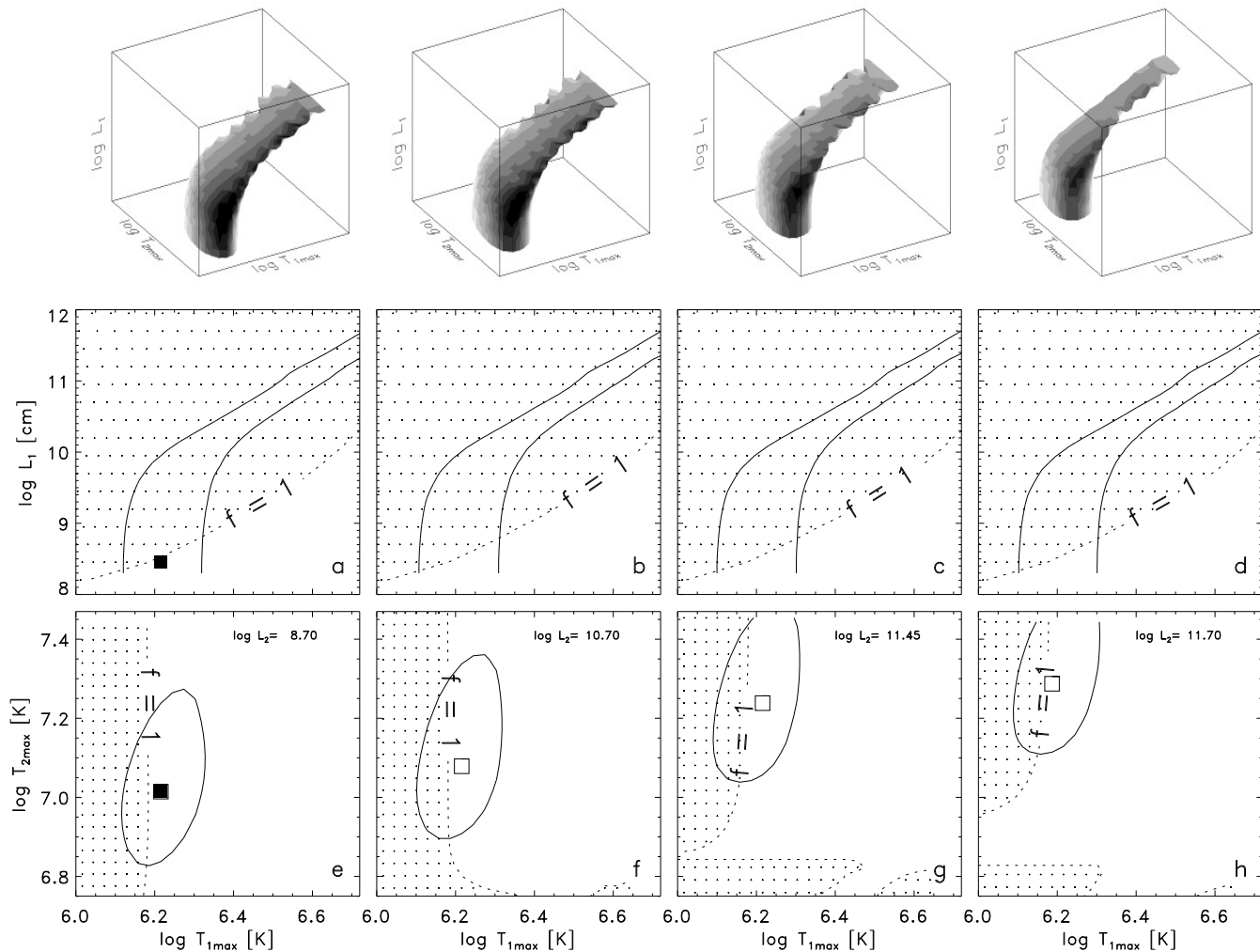


Fig. 7a-h. 90% χ^2 confidence regions in the $T_{1\max}$ - $T_{2\max}$ - L_1 space, at four fixed values of L_2 (5×10^8 , 5×10^{10} , 2.8×10^{11} , 5×10^{11} cm), for the 2-loop model analysis of HR 3625. The figures in the top row show the 3-D confidence region, which moves almost rigidly in the direction of increasing $T_{2\max}$, for increasing L_2 . The axis closest to horizontal is in the $T_{1\max}$ direction, while L_1 increases along the vertical axis of the image. **a-d** show cross sections of the 3-D confidence regions, in the $T_{1\max}$ - L_1 plane, at fixed $T_{2\max}$ values corresponding to the minimum χ^2 location (shown as a square symbol in the corresponding lower panel) within each 3-D confidence region. In **e-h**, we show cross sections of the 3-D confidence regions, in the $T_{1\max}$ - $T_{2\max}$ plane, all at the same L_1 value, the one of the best-fit model. The filled square marks the global χ^2 minimum (best-fit model); the empty squares, instead, the minimum χ^2 location within each 3-D confidence region

the emission is assumed to come from a magnetically-confined corona and the characteristics of the coronal structures are inferred by interpreting the fitting results (in particular, temperatures and fluxes) in terms of the scaling laws for isobaric loops (Rosner et al. 1978). The latter indirect approach has some limitations: it does not guarantee that the actual, detailed loop model spectra, if computed with the parameters derived from the scaling laws, provide an acceptable fit to the observed spectra; for ease of computation, the loops are usually assumed isobaric, thus excluding possible solutions with loops comparable to the pressure scale height or longer; if the fitting is performed with 2-T models, as in Giampapa et al. (1996), since the arguable correspondence between the 2-T model parameters (temperatures and emission measures of the two components) and the 2-loop model parameters (temperatures, lengths and filling fac-

tors) is not unique³, some assumption must be made, e.g., on the surface filling factors, in order to derive the other loop parameters; in the other case, if an emission measure with a power-law distribution is the model assumed, as in Preibisch (1996), the three fitted parameters (slope, maximum temperature and normalization) can be used to guess one-loop parameters, but not two-loop solutions; moreover, detailed confidence regions in the loop model parameter space cannot be easily evaluated. Finally, as a note of caution in interpreting the results obtained with such indirect approaches, we note that the temperatures derived from 2-T model fitting, are average plasma temperatures, weighted by the source spectrum convolved with the instrument response,

³ Note that 2-T models need four parameters, while 2-loop models need six parameters.

and they cannot be directly interpreted as the maximum plasma temperature in closed coronal structures (see Paper I and II). Indeed, a one-component thermal fitting of a loop spectrum invariably leads to a temperature significantly lower than T_{\max} , because of the intrinsic averaging effect of the instrument (Paper III). For all the above reasons, we have preferred to pursue the approach of the direct loop model fitting, which compensates the relatively larger computational difficulty with the significance and reliability of its results and its diagnostic power. The examples presented in this paper make us confident that loop model fitting, applied to ROSAT, ASCA and SAX data, would provide with an interpretation of stellar coronal emission more detailed than with other methods.

Acknowledgements. The authors acknowledge partial support from Ministero dell'Università e della Ricerca Scientifica e Tecnologica, the Italian Space Agency, and GNA-CNR. They also acknowledge the stimulus by Prof. S. Serio to pursue the two-loop modeling of stellar coronal emission, and discussion and suggestions from Dr. J. Pye, Dr. R. Ventura, Dr. F. Reale, Dr. S. Sciortino, and Dr. G. Micela.

References

- Allen C.W. 1973, *Astrophysical Quantities* (3rd edition). Athlone, London
- Anders E., Grevesse N. 1989, *Geochimica et Cosmochimica Acta* 53, 197
- Barnes T.G., Evans D.S., Moffett T.J. 1978, *MNRAS* 183, 285
- Bocchino, F., Maggio, A., Sciortino, S. 1994, *ApJ* 437, 209
- Ciaravella A., Peres G., Maggio A., Serio S. 1996, *A&A*, 306, 553 (Paper I)
- Ciaravella A., Maggio A., Peres G. 1997, *A&A*, in press (Paper III)
- Drake J.J., Laming J.M., Widing K.G. 1995, *ApJ* 443, 393
- Fiore F., Elvis M., Siemiginowska A., Wilkes B.J., McDowell J.C. 1994, *ApJ* 431, 515
- Gehrels N. 1986, *ApJ* 303, 336
- Giampapa M.S., Rosner R., Kashyap V., Fleming T.A., Schmitt J.H.M.M., Bookbinder J.A. 1996, *ApJ* 463, 707
- Gilliland, R.L. 1985, *ApJ*, 299, 286
- Jordan C. 1996, In: Bowyer S., Malina R. (eds.) *Proc. IAU Coll. no. 152, Astrophysics in the Extreme Ultraviolet*. Kluwer, Dordrecht, p. 81
- Jordan C., Brown A., Walter F.M., Linsky J.L. 1986, *MNRAS* 218, 465
- Lampton M., Margon B., Bowyer S. 1976, *ApJ* 208, 177
- Lemen J.R., Mewe R., Schrijver C.J., Fludra A., 1989, *ApJ* 341, 474
- Maeder A., Meynet G. 1988, *A&AS* 76, 411
- Maggio A., Peres G. 1996, *A&A*, 306, 563 (Paper II)
- Maggio A., Reale, F., Peres, G., Ciaravella, A. 1994a, *CPC*, 81, 105
- Maggio A., Sciortino S., Harnden F.R., Jr. 1994b, *ApJ*, 432, 701
- Preibisch T., 1997, *A&A*, in press
- Paresce F. 1984, *AJ* 89, 1022
- Press W.H., Flannery B.P., Teukolsky S.A., Vetterling W.T. 1986, *Numerical Recipes*, Cambridge University Press
- Raymond J.C., Smith B.W. 1977, *ApJS*, 35, 419
- Rosner R., Tucker W.H., Vaiana G.S. 1978, *ApJ* 220, 643
- Serio S. 1995, In: Uchida Y., Kosugi T., Hudson H.S. (eds.) *Magnetodynamic Phenomena in the Solar Atmosphere*. Kluwer, Dordrecht, p. 63
- Serio S., Peres G., Vaiana G.S., Golub L., Rosner R. 1981, *ApJ* 243, 288
- Schmitt J.H.M.M. 1990, *Adv. Space Res.* 10, 115
- Schmitt J.H.M.M., Harnden F.R., Jr., Peres G., Rosner R., Serio S. 1985, *ApJ* 288, 751
- Schmitt J.H.M.M., Haisch B.M., Drake J.J. 1994, *Science* 265, 1420
- Schmitt J.H.M.M., Drake J.J., Haisch B.M., Stern R.A. 1996, *ApJ* 467, 841
- Schrijver C.J., Mewe R., Van den Oord G.H.J., Kaastra J.S. 1995, *A&A* 302, 438